Intraband transitions between bulk states of Cu(100) probed with threshold two-photon photoemission

Ann Author* and Second Author†
Authors' institution and/or address
*This line break forced with *

Charlie Author‡
Second institution and/or address
This line break forced
(Dated: February 14, 2015)

An article usually includes an abstract, a concise summary of the work covered at length in the main body of the article. It is used for secondary publications and for information retrieval purposes. Valid PACS numbers may be entered using the `\pacs{#1}` command.

PACS numbers: 73.20.At; 79.60.Bm; 42.62.Fi

I. INTRODUCTION

Angle-resolved photoemission (ARPES) has been the workhorse spectroscopy for the understanding of the electronic structure of bulk and surface of clean and covered surfaces[1]. It offers information of the occupied bands below the Fermi energy E_F and the nonoccupied ones above the vacuum level E_{vac}. Spectroscopic information of empty bands below E_{vac} can be obtained from inverse photoemission spectrocopy (IPES) but the low resolution of this technique makes sometimes difficult to extract information from spectrum [2]. Two-photon photoemission spectroscopy (2PPES) is a suitable technique for studying the electronic structure and dynamics of excited states of metals and semiconductors below E_{vac}[3].

The identification of bulk band transitions in 2PPES can be difficult thus is a surface sensitive technique. There are not many reports in the literature that involve bulk states. We can mention the study of transitions between bulk bands of Si(100)[4] or the identification of a saddle point in the band structure of graphite[5]. For metals it worth to mention the early work of Giesen et al.[6] were an unoccupied bulk state was identified for Ag(111). This result was reinterpreted as a transition between two sp-bands[7]. In metals there is just one report of 2PPE from a bulk unoccupied state. In this study Wegehaupt et al.[8] presented results concerning an interband transition between the occupied state X_5 and the unoccupied $X_4^{'}$ on Cu(100) was characterized.

Transitions between bulk bands can be realized through k-conserving direct interband transitions or through k-nonconserving intraband transitions. Intraband transitions from for example an occupied sp-state to an unoccupied sp-state from the same band are possible by momentum contribution due to a scattering process by defects, impurities or phonons. Under the framework of femtosecond pulses, the difference of lifetime of photoelectrons has been measured and compared for intraband and interband transitions in the Cs/Cu(111) system[9].

The electron band structure of copper is, perhaps the best known among the metals[10]. However as it was point out recently by Fauster [11], the agreement between experiment and bulk band structure calculations is far from perfect. Meanwhile there is a good agrement among different experimental results and theoretical calculations for unoccupied states as the image states[12] the situations is not the same for the empty bulk states in the interval of energies between E_F and E_{vac}. Just to mention, the difference in energy between the latest results for the energy assignment for $X_4^{'}$ in Cu taking into account the experimental uncertainty is over half eV[8, 13].

To the best of our knowledge we report the first intraband transition between sp-states of Cu probed by energy-resolved 2PEE on Cu(100). The study was performed with photon energies slightly higher than half of the Cu(100) work function where the threshold 2-photon photoemission (Th-2PPE) is expected. The intermediate unoccupied state for the 2-photon process corresponds with the high symmetry point $X_4^{'}$. A study of the population of this state as a function of temperature was performed and a theoretical description of the process is offered. As a result, the position in energy of the bulk state $X_4^{'}$ is given with high accuracy.

II. EXPERIMENT

The experimental setup has been described in a recent publication and will be briefly described here [14]. The experiments were carried out under Ultra-High-Vacuum (UHV) conditions and room temperature on a Cu(100) crystal which was cleaned following standard procedures. For electron and ion detection some home-made components were installed into the UHV chamber, such as a

*Also at Physics Department, XYZ University.
†Electronic address: Second.Author@institution.edu
‡URL: http://www.Second.institution.edu/~Charlie.Author

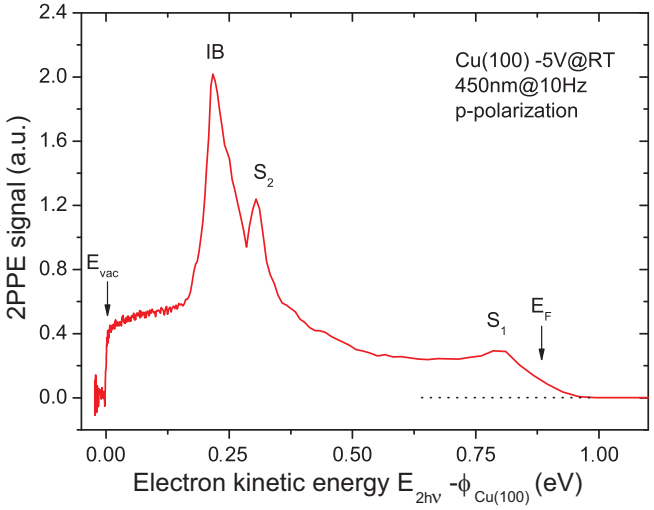

FIG. 1: Two-photon photoelectron distribution generated by p-polarized light and 450 nm laser wavelength. Three peaks are showed: IB assigned as the intraband transition, a second peak close to IB named as S_2 and a third peak close to the Fermi energy named as S_1.

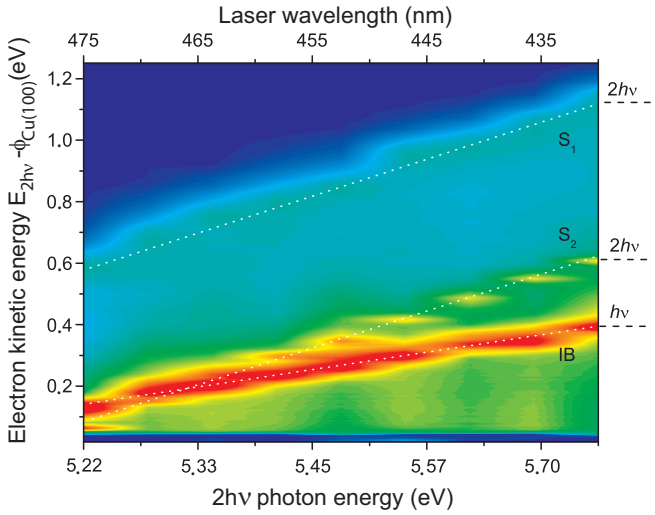

FIG. 2: Contour plot of the 2PPE spectra as a function of the photon energy of the laser with p polarization. The Cu(100) sample was kept at 295 K and biased with -5 V. The behavior of the three peaks IB, S_1 and S_2 were lineal and consistent with one, two and two photon processes respectively.

rotateable hemispherical electron analyzer and a time-of-flight mass spectrometer.

The laser system consists of a Nd:YAG laser (Coherent Infinity) delivering pulses with a temporal width of 3 ns and repetition rate between 0.1 and 30 Hz. The fundamental output of the Nd:YAG is frequency tripled (355 nm) by two non-linear crystals and directed into an optical parametric oscillator (Coherent XPO). By changing the angle of incidence of the incoming beam with respect to the non-linear crystal Beta Barium Borate (BBO) pulses between 1 and 15 mJ energy, 3 ns duration and s-polarization were provided. The laser wavelength was tuneable between 420 nm and 650 nm (2.95-1.91 eV photon energy) and transversal mode with hat top profile could be generated with a homogeneous power density on the sample bellow $1{\cdot}10^5$ MW/cm^2 to avoid space charge effects.

The laser polarization was rotated to p-polarization by a periscope and the purity of the polarization increased by a Glan-Taylor polarizer (Thorlabs GL5). Beam divergence was adapted by a Galilean telescope and pulse energy adjusted by a variable attenuator (Newport M-935-5-OPT) down to 0.1 % of the incoming beam energy. The angle of incidence of the laser beam with respect to the normal of the sample was 45 degrees.

Electron distributions generated by the focused laser beam were analyzed normal to the sample surface by a 300 mm time-of-flight mass spectrometer and detected by a dual microchannel plates (MCP).

III. EXPERIMENTAL RESULTS

Surface irradiation by nanosecond laser pulses under ThPES regime at room temperature guarantees (a) thermal equilibrium between the electrons and the lattice, (b) that electron-phonon will be the dominant contribution to electron scattering and (c) that Drude model can be applied in this case, being the electron-phonon collisional frequency proportional to the lattice temperature.

As a first application we show how ThPES allows high precision measurements of the electron band structure of the sample. Figure 1 shows a typical 2PPE spectrum using p-polarized light and 450 nm laser wavelength (2.75 eV photon energy) and -5V bias applied to the surface. Under these experimental conditions an electron distribution with a total width of 0.91 eV was measured, value which is in good accordance with previous Cu(100) work function values[15]. The low energy cutoff suggests a 60 meV resolution for the electron spectrometer.

Two main peaks are observed in Figure 1 corresponding with 256 meV and 346 meV energies named as IB and S_2 respectively. A third weak structure, named as S_1 is identified close to the Fermi energy.

The electron signal was monitored by tunning the laser wavelength from 475 down to 430 nm while mantaining the rest of the experimental parameters constant. Figure 2 shows the electron signal as a surface plot where hot colours (red) represent higher signal, while cold colours (blue) smaller. The upper horizontal axis represents the laser wavelength in nm and the lower one the correspondent energy for a two photon process in eV. The vertical axis represents the kinetic energy of the photoemited electrons in eV. A linear behavior with a 0.47 slope was measured by increasing the energy per laser photon for

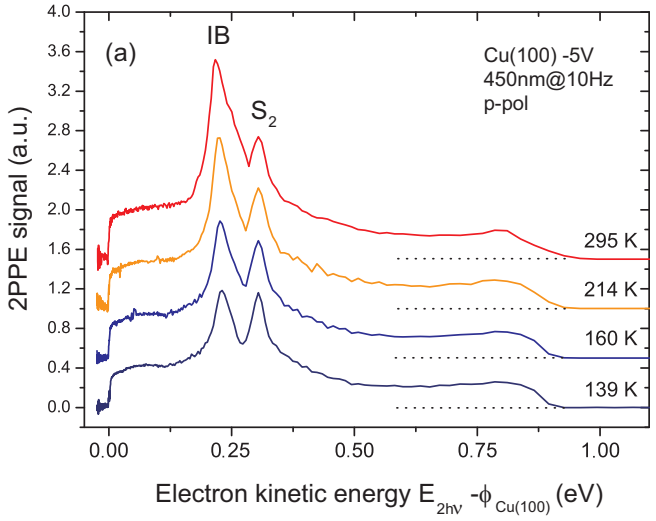

FIG. 3: Two-photon photoelectron distribution generated by p-polarized light and 450 nm laser wavelength as a function of the sample temperature: 295 K (red), 214 K (yellow), 160 K (blue) and 139 K (violet).

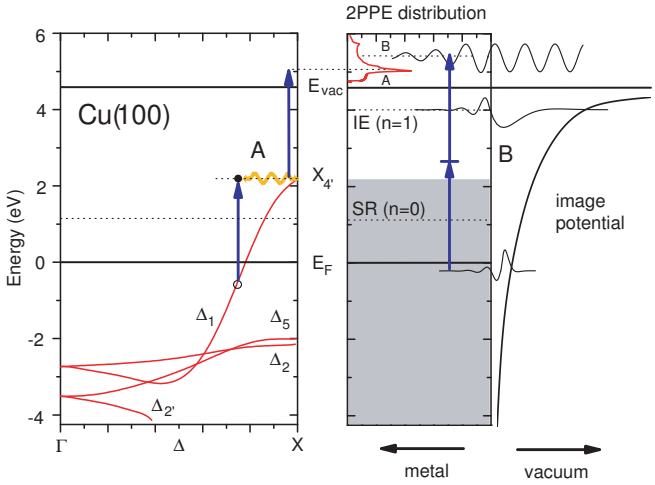

FIG. 4: (Left) Band structure of Cu(100) calculated according to Ref. [16]is shown as red solid lines. Horizontal axis indicate the perpendicular momentum. (Right)Dashed lines show the occupied and unoccupied surface states and resonances. The vertical arrows named as A represent the intraband transition where the intermediate state is $X_{4'}$. The vertical arrows named as B represent the rest of transitions (including S_1 and S_2) where a virtual stated acts as intermediate state.

the IB peak, consistent with one photon process. A second trace with a 0.91 slope was measured for the S_2 peak which crosses the IB one for a 2hν value of 5.33 eV. The behavior of the third small peak S_1 was also lineal when varying the laser wavelegnth with a 1.15 slope value. Thus the behavior of both peaks S_1 and S_2 were consistent with a two photon process.

To study the effect of temperature in the electron signal, the sample was cooled from RT down to 139K. Figure 3 shows four photoelectron spectra as function of tempeture T= 295, 214, 160 and 139K with an offset for clarity. By decreasing the surface temperature, is noticeable a clear change in the slope of the Fermi tail in the high energy part of the electron distribution, as well as a decrease of the secondary electron signal close to 0 eV and the IB peak, with a reduction down to 56% of its area. However, it can be seen that the intensity of the S_2 is constant under these conditions.

Whereas the high energy peak is originated by coherent 2PPE from bulk states, the low energy one is due to non-coherent intraband transitions from sp band. Is remarkable the absence of secondary electron emission in the spectrum due to the purity of the p-polarization of the light and the low laser power density used in the experiments.

By increasing the laser wavelength, the photon energy is not enough to generate strong transitions from symmetry points. Figure 5 shows an electron spectrum using p-polarization and 490 nm (2.53 eV per photon) and the same power density as in Figure 3. Only a weak signal can be detected from the continuum of the copper bulk bands. A more detailed study is now in progress in our laboratory to investigate the dynamics of these intraband transitions and will be the subject of a future paper.

IV. CALCULATION OF ENERGY-RESOLVED TWO-PHOTON PHOTOEMISSION SPECTRA

V. DISCUSSION

Figure 4 displays the basis for discussion of 2PPE where the electronic band structure of Cu(100) is shown according to the calculation of Burdick [16].

The visible absorption spectrum of copper consists of absorption with a threshold of ≈-2.0 eV beeing the main excitation process interband transitions from near the top of the d-bands starting at -2 eV to the sp-band. For a two-photon process with hν between 2.61 and 2.88 eV, it will create a hot-electron distribution with a range of energies between E_F and but no photoelectron over E_{vac}.

For Cu(100) the lowest image state (IS, n=1) is situated 0.53 eV below the vacuum level [17]. This surface-induced electron state can be populated by the absorption of two photons; however, the photocurrent can not overcome the vacuum level. The same argument can be invoked to disregard photoemission from the surface resonance state (SR) 1.1 eV above the Fermi level E_F [18].

Vertical excitation from the sp-band of the electron-hole pair is possible through a virtual state if a second photon is absorbed before the electron-hole pair can decohere as in shown in the B mechanism of Figure 4. This coherent 2PPE lead to a flat continuum in the electron signal.

Since saddle point $X_{4'}$ corresponds to peaks in the DOS one can expect that strong transitions will take place from occupied states below the E_F to states near $X_{4'}$ as Berglund and Spicer pointed out [19]. As shown

in Figure 4, the sp-band of Cu has some similarity to a nearly free-electron band. Thus, optical intraband excitations are, in general, not possible. Intraband transitions from an occupied sp state to an unoccupied sp state of the same band are only possible by momentum transfer mainly due to phonon scattering processes and, up to a certain extent, to scattering by defects and impurities. However the temperature dependence of free electron absorption in noble metals indicates that the phonon scattering is the dominant mechanism [20]. Figure 4(a) shows this incoherent process, marked with A, where the phase between the electron and its hole is lost and the $X_{4'}$ is populated as intermediate state of the 2PPE process. A detailed analysis of the intraband transition peak (marked with A in the Figure 3) and the signal from sp-band (marked with an arrow in Figure 3) shows a B/A branching ratio of X.

This ratio can be explained taking into account that the incoherent 2PPE process A is mediated through a real state with high density of empty states in comparison with the coherent process B where the intermediate state is a virtual state with transition probability significantly smaller than A.

The value of the energy of $X_{4'}$ is of special interest for nonocuppied states of the sp band in the Γ momentum direction. In a very interesting IPES work on Cu(100) and k$^{\ll}$=0 Himpsel et al.[13] measured firts IS n=1 and n=2 as well as a structure centered at 1.4 eV that they identified as a surface resonance (SR). Finally the $X_{4'}$ was identified at 1.8 eV poorly resolved as the inflexion point of the signal tail for values close to 2 eV.

An interband transition between volume states d→sp was measured by 2PPE by Wegehaupt et al. [8] for Cu(100) and the $X_{4'}$ state was identified and energetically evaluated at 1.48±0.06 eV, in accordance with DFT calculations [21]. However, these results were reinterpret by Himsel et al. as a transition from d bands to the n=0 SR. Thus, we present the first 2PPE measurements of $X_{4'}$. Energy balance applied to the intraband peak location indicates that the $X_{4'}$ point appears to be located at 2.08 eV above E_F value, in good agreement with the predictions of local-density calculations [22] and previous measurements [13]. The presence of the high energy peak is also consistent with the existence of a region of highly localized states below E_F that we identify as the $L_{2'}$ point situated in the ΓL symmetry line.

State S_1 was measured X eV below the Fermi Energy and is identified with a Shockley state first reported in $\bar{X}$ at 0.06 binding energy [23] and more recently at 0.05 eV by Baldacchini et al. [24]. State S_2 was measured at X eV below Fermi Energy level and is identified with a surface state reported at 0.75 eV [24] binding energy in $\bar{X}$. Both states were confirmed by recent ARUPS measurements along $\bar{X}$-$\bar{M}$ direction [25]

TABLE I: This is a narrow table which fits into a narrow column when using `twocolumn` formatting. Note that REVTEX 4 adjusts the intercolumn spacing so that the table fills the entire width of the column. Table captions are numbered automatically. This table illustrates left-aligned, centered, and right-aligned columns.

Left[a]	Centered[b]	Right
1	2	3
10	20	30
100	200	300

[a]Note a.
[b]Note b.

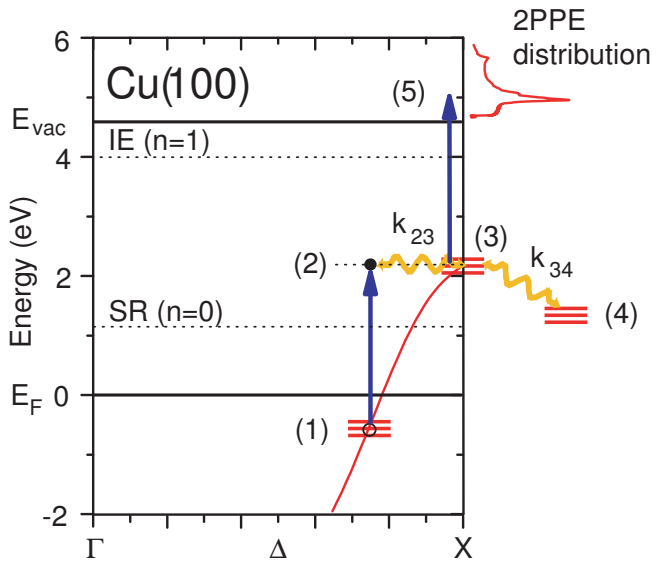

FIG. 5: Two-photon photoelectron distribution generated by p-polarized light and 450 nm laser wavelength. Intraband transition peak is marked with A and the coherent transition peak is marked as B.

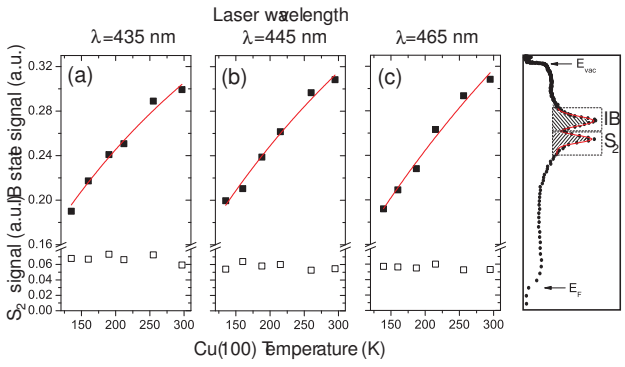

FIG. 6: Two-photon photoelectron distribution generated by p-polarized light and 450 nm laser wavelength. Intraband transition peak is marked with A and the coherent transition peak is marked as B.

VI. THEORETICAL MODEL

VII. CONCLUSIONS

Acknowledgments

We wish to acknowledge the support of the author community in using REVTEX, offering suggestions and encouragement, testing new versions, ...

APPENDIX A: APPENDIXES

To start the appendixes, use the `\appendix` command. This signals that all following section commands refer to appendixes instead of regular sections. Therefore, the `\appendix` command should be used only once—to setup the section commands to act as appendixes. Thereafter normal section commands are used. The heading for a section can be left empty. For example,

```
\appendix
\section{}
```

will produce an appendix heading that says "APPENDIX A" and

```
\appendix
\section{Background}
```

will produce an appendix heading that says "APPENDIX A: BACKGROUND" (note that the colon is set automatically).

If there is only one appendix, then the letter "A" should not appear. This is suppressed by using the star version of the appendix command (`\appendix*` in the place of `\appendix`).

APPENDIX B: A LITTLE MORE ON APPENDIXES

Observe that this appendix was started by using

```
\section{A little more on appendixes}
```

Note the equation number in an appendix:

$$E = mc^2. \tag{B1}$$

1. A subsection in an appendix

You can use a subsection or subsubsection in an appendix. Note the numbering: we are now in Appendix B 1.

Note the equation numbers in this appendix, produced with the subequations environment:

$$E = mc, \tag{B2a}$$
$$E = mc^2, \tag{B2b}$$
$$E \gtrsim mc^3. \tag{B2c}$$

They turn out to be Eqs. (B2a), (B2b), and (B2c).

[1] ARPES, Book/review about ARPES **37**, 10086 (1988).
[2] IPES, Book/review about IPES **37**, 10086 (1988).
[3] 2PPES, Book/review about 2PPES **37**, 10086 (1988).
[4] C. Kentsch, M. Kutschera, M. Weinelt, T. Fauster, and M. Rohlfing, Phys. Rev. B **65**, 035323 (2002).
[5] G. Moos, C. Gahl, R. Fasel, M. Wolf, and T. Hertel, Phys. Rev. Lett. **87**, 267402 (2001).
[6] K. Giesen, F. Hage, F. Himpsel, H. Riess, and W. Steinmann, Phys. Rev. Lett. **55**, 300 (1985).
[7] S. Pawlik, R. Burgermeister, M. Bauer, and M. Aeschlimann, Surf. Sci. **402-404**, 556 (1998).
[8] T. Wegehaupt, D. Rieger, and W. Steinmann, Phys. Rev. B **37**, 10086 (1988).
[9] S. Pawlik, M. Bauer, and M. Aeschlimann, Surf. Sci. **377-379**, 206 (1997).
[10] Hufner, Book of PES from Hufner **377-379**, 206 (1997).
[11] T. Fauster, Book of 2PPE from Th. Fauster **377-379**, 206 (1997).
[12] IS, Book/review about IS **37**, 10086 (1988).
[13] F. Himpsel and J. Ortega, Phys. Rev. B **46**, 9719 (1992).
[14] J. Tornero, H. Telle, G. Garca, and A. G. U. na, Phys. Chem. Chem. Phys. **13**, 8475 (2011).
[15] P. Gartland, S. Berge, and B. Slagsvold, Phys. Rev. Lett. **28**, 738 (1972).
[16] G. Burdick, Phys. Rev. **129**, 138 (1963).
[17] K. Giesen, F. Hage, F. Himpsel, H. Riess, and W. Steinmann, Phys. Rev. B **35**, 971 (1987).
[18] A. Goldmann, V. Dose, and G. Borstel, Phys. Rev. B **32**, 1971 (1985).
[19] C. Berglund and W. Spicer, Phys. Rev. **136**, A1030 (1964).
[20] K. Kliewer and K. Bennemann, Phys. Rev. B **15**, 3731 (1977).
[21] A. Kheifets, D. Lun, and S. Savrasov, J. Phys.: Condens. Matter **11**, 6779 (1999).
[22] H. Eckardt, L. Fritsche, and J. Noffke, J. Phys. F **14**, 97 (1984).
[23] S. Kevan, Phys. Rev. B **28**, 2268 (1983).
[24] C. Baldacchini, L. Chiodo, F. Allegretti, C. Mariani, M. Betti, P. Monachesi, and R. del Sole, Phys. Rev. B **68**, 195109 (2003).
[25] D. Sekiba, F. Komori, and P. Cortona, Phys. Rev. B **75**, 165410 (2007).